Article

Dynamic In-Situ Observation on the Failure Mechanism of Flax Fiber through Scanning Electron Microscopy

Shabbir Ahmed and Chad A. Ulven *

Department of Mechanical Engineering, North Dakota State University, Fargo, ND 58102, USA; shabbir.ahmed@ndsu.edu
* Correspondence: chad.ulven@ndsu.edu; Tel.: +1-701-231-5641

Abstract: In order to develop and improve bio-inspired fibers, it is necessary to have a proper understanding of the fracture behavior of bio-fibers such as flax fibers from an individual fiber down to the constituent micro-fibrils and nano-fibrils. For investigating the failure mechanism of individual and technical flax fibers, a tensile test bench was placed within a scanning electron microscope, and the entire process of fiber failure was investigated through the capture of an SEM movie. Next, fractographic analysis was performed on the failure surface of single fibers as well as meso-fibrils that failed at a displacement rate of 0.25 mm/min, 0.75 mm/min, and 1.6 mm/min. The analysis also enabled visualization of a few internal details of flax fiber such as the arrangement of meso-fibrils and micro-fibrils (nano-fibrils). It was shown that the crack bridging mechanism and successive fiber pull-out contributed to the high work of fracture of flax fiber and the value may reach as high as 10^6 J/m^2.

Keywords: flax fiber; fractography; failure mechanism; SEM; crack bridge; single fiber; technical fiber

1. Introduction

Flax fibers are an attractive choice for utilization in advanced polymer matrix composite materials as reinforcing agents due to their lighter weight and lesser dermal abrasion characteristics, reduced energy requirement during processing, better vibration dampening characteristics, better insulation, and sound absorption capabilities compared to the petroleum based/synthetic fibers [1]. Although flax fibers lack many of the impressive properties of synthetic fibers such as higher uniformity, higher strength, thermal stability and non-flammability, their characteristic biodegradability, moderate mechanical properties, and non-toxic nature have outweighed these shortcomings in certain applications [2].

The typical diameter of an elementary fiber varies from 10–15 μm and a few elementary fibers are grouped together to form a technical fiber [3]. Typically, the diameter of technical fibers vary between 35–150 μm (Figure 1) [4].

(**a**) (**b**)
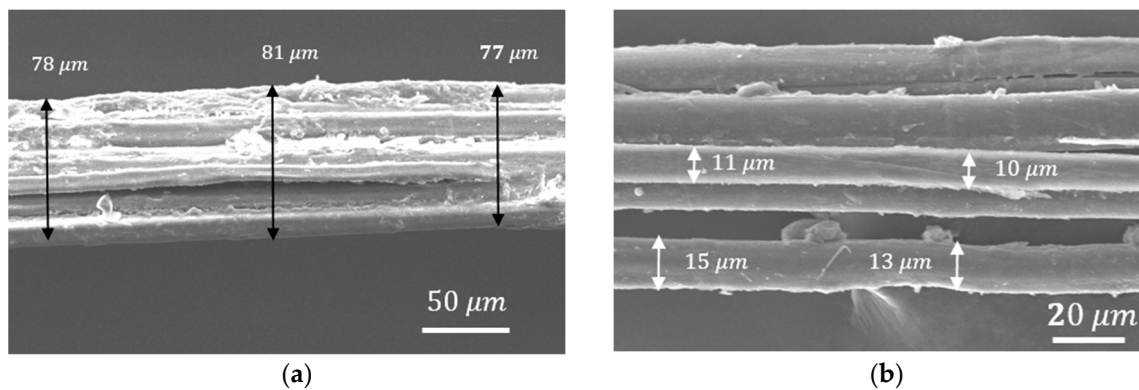
Figure 1. (**a**) Technical fiber: several individual cells bonded together by pectin; (**b**) Single fiber: individual sclerenchyma cells, and diameter varies between 10–15 micrometer.

Elementary fibers are essentially multinucleate single elongated sclerenchyma cells [5]. These elementary fibers are not uniform monofilaments like glass or carbon fibers, rather they are layered structure and a composite in itself. Flax fibers also have a hollow interior, which is called a lumen. However, in mature flax the lumen tends to be very small [6]. A flax fiber cell wall is comprised of two individual walls: the primary wall and the secondary wall. The primary wall is a single layer with a thickness of around 0.2 μm and it consists mainly of cellulose, hemicelluloses (xyloglucan and/or glucomannan) and pectic polysaccharides [7,8]. Lignin is present only in the secondary wall and it is deposited on the preexisting [9] polysaccharide matrix of cellulose and hemicellulose [10]. The secondary wall generally has three layers namely S1, S2 and S3 with a thickness of 0.5–2 μm, 5–10 μm and 0.5–1 μm respectively [2,11,12]. Among them the S2 layer is the thickest and around 70% of the Young's Modulus is mainly governed from this part of the structure [13]. The formation of these different layers occurs during the growth stage of bast fibers, more specifically, when the elongation of the cell stops and the thickening of the cell wall begins. The inner part of the developing cell wall is called the galactan enriched matrix or Gn-layer. The outer part is known as the G-layer. This G-layer is also known as the S2 layer of flax fiber cell wall [14]. G-layer is much more homogeneous than Gn-layer, and as the secondary cell wall development proceeds, Gn-layer gradually transforms into G-layer [15,16]. At fiber maturity, all of the Gn-layer is converted into G-layer. During this conversion process from Gn-layer to G-layer, it is possible that additional layer or strata may have created in the mature flax fiber cell wall. The transmission electron microscopy of mature flax fiber cell wall suggests that the conventional four layer model (P/S1/S2 or G-layer/S3) is not accurate enough to represent flax fiber cell wall as there are more than four layers present in the cell wall [13].

The S2 layer is analogous to a composite lamina where cellulose meso-fibrils, having a diameter of 100–200 nm, are helically arranged in an amorphous matrix of hemicellulose and pectin (Figure 2) [3]. The meso-fibrils are a bundle of microfibrils having a diameter between 2–10 nm [17,18]. These fibrils are at an angle with the fiber longitudinal direction, known as the helix angle or microfibril angle of the fibrils. Astley et al. [19] measured the helix angle of flax fiber with small angle X-ray diffraction technique and investigated the effect of water sorption on microfibril angle. In dry state the angle is approximately 10° and in wet state the angle is 15°. This angle is quite small when compared to the helix angle of cotton fibers (30°) and coir and some leaf fibers (more than 40°) [20–22].
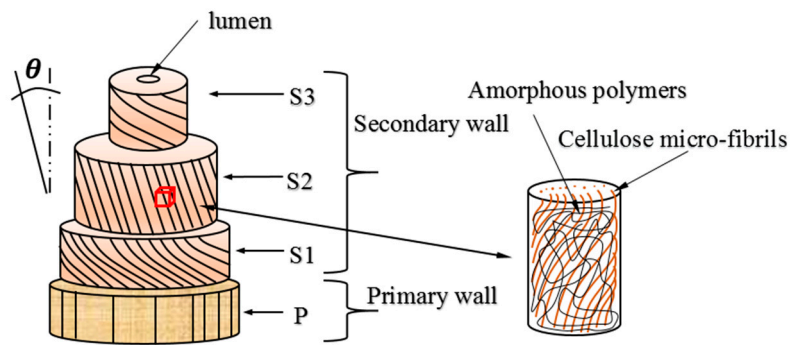
Figure 2. Schematic diagram of a single fiber with primary and secondary layers, secondary layer is composed of S1, S2, and S3 layer. A smaller portion of S2 layer is magnified and cellulose micro-fibrils are seen to be dispersed on an amorphous polymeric matrix. Concept adapted from [12].

The failure strength and failure strain of flax fibers have been investigated widely [12,23–26]. The compressive strength of flax fiber is about 80% of its tensile strength whereas polymeric or glass fiber has much lower compressive strength, about 20% of the tensile strength [24]. Andersons et al. [27] investigated the effect of mechanical defects on the strength distribution of elementary flax fibers. He proposed that a modified Weibull distribution instead of a two-parameter Weibull distribution can approximate the strength with greater accuracy. McLaughlin et al. [28] studied the fracture mechanism of different plant fibers by SEM micrograph and tensile testing of single cells and found that the work of fracture depends on the helix angle as well as the cellulose content of the fiber. Nilsson et al. [29] studied the influence of dislocations on the tensile behavior of flax and hemp fibers by finite element analysis. They assumed the elementary flax fiber as a thick walled cylinder and modeled only the secondary layer. For simplicity of analysis, a circular cross-section was assumed and it was considered that cellulose micro-fibrils are embedded in a hemicellulose matrix. The effect of lignin and pectin were neglected. Thygesen et al. [30] studied the effect of growth and storage conditions on the distribution of dislocations on hemp fibers. They found that the dislocations are present in the fiber even before harvest and mechanical isolation. Different growing conditions such as wind and aridity were found to produce similar effects on dislocations. The storage of fiber in different moisture conditions also affects the presence of dislocations. They also indicated that these dislocations tend to reduce the strength of fibers. Davies and Bruce [31] studied the effect of damage or dislocations and relative humidity on the tensile properties and stiffness of flax fibers. They observed that the overall effect of damage was to decrease the tensile strength and stiffness of flax fiber. They mentioned that the relative humidity did not have much influence on the tensile strength but decreases the stiffness of flax fiber. Bos et al. [32] investigated the fracture surface of elementary fibers by straining a loop of elementary fiber. He showed that failure in primary wall is brittle, whereas in secondary wall crack bridging occurs. Mott et al. [33] performed the in-situ tensile testing of single wood fibers. However, to the author's knowledge, no study has been performed analyzing the dynamic failure of flax fiber in tension. Very little images are available in the literature studying the cross-sectional fracture surface of flax fibers. To remedy this shortcoming, in-situ observation on the failure mechanism of technical and elementary flax fibers have been investigated in the present study. The elusive mesofibrils residing in the secondary layer and their helical arrangement, i.e., microfibril angle were made visible in their natural state.

It has been a constant source of confusion in the literature about the dimension of mesofibrils and microfibrils of flax fibers. Sometimes, the dimension of mesofibrils and microfibrils of single wood fibers are interchangeably used with flax fibers. In this study, fibrils with approximately 0.5–1 μm have been referred to as meso-fibrils [34]. Fibrils with 30–70 nm have been referred to as microfibrils.

2. Materials and Methods

Flax fibers used in this study were linseed flax, provided by Composite Innovation Center (CIC), Winnipeg, Canada. The technical fibers were carefully hand separated for tensile testing. The diameters of the fibers were measured by a Zeiss Axiovert 40MAT inverted optical microscope. The diameter was measured at three different locations of the fiber and then the averaged.

For performing the tensile tests, ASTM standard D3822/D3822M was followed. The tensile testing was performed with a Deben Microtest tensile test bench with a maximum load cell capacity of 180 N. The fibers were clamped at both ends of the machine. The gauge length of the fibers was fixed at 20 mm with displacement rates of 0.25 mm/min, 0.75 mm/min, and 1.6 mm/min. At least 50 fibers were tested outside the SEM with each of the three displacement rates for evaluating the strength, strain and Young's modulus on a statistical basis (a total of 150 fibers at least). For dynamically investigating the failure mechanism of flax fiber, the tensile test bench was placed inside the scanning electron microscopy (JEOL JSM-6490LV high performance variable pressure SEM) and three fibers were tested in-situ. With the help of the SEM imaging system, movies were recorded over periods of 1 min while the fiber was being pulled in tension, until the failure of the fibers occurred. The speed of the imaging system was 30 frames/second.

Next, 10 technical fibers were again tested and field emission scanning electron microscopy (FESEM) (JEOL JSM-7600F scanning electron microscope, JEOL USA Inc., Peabody, MA, USA) was used (for higher resolution) to investigate the fractured surface of the fibers that failed at three different displacement rates: 0.25 mm/min, 0.75 mm/min, and 1.6 mm/min. The fractured samples were carefully mounted on aluminum mounts using carbon tabs and then coated with a conductive layer of carbon in a high-vacuum evaporative coater (Cressington 208c, Ted Pella Inc., Redding, CA, USA).

3. Results and Discussion

In Figure 3a, the force-elongation curve for one of the technical flax fibers tested is shown (one representative figure out of 150 fibers). The area under this curve represents the total energy absorbed during the fracture and it is calculated to be 0.2956 N-mm. Figure 3b shows the viscoelastic nature of one of the technical flax fibers tested. This curve was generated by successive loading and unloading of a single technical fiber with a diameter of 110 μm (representative one). This was a displacement control test. For cycle 2, unloading was performed at a strain when the stress of cycle 2 exceeded cycle 1. Again, for cycle 4, unloading was performed at a strain when the stress of cycle 4 exceeded cycle 3. For cycle 2, less strain was required to exceed 120 MPa (stress of cycle 1) as the slope of cycle 2 was higher than the cycle 1. Similar trend was observed in cycle 3 and 4. For cycle 1, the slope of the loading curve is lower than the unloading curve, that is, the modulus increases after the fiber is strained. The area enclosed by the loading-unloading curve represents the hysteresis loss of the cycle. In cycle 2, 3 and 4 the slope of the loading and the unloading curve is almost similar. However, with each successive cycle the slope of the loading curve gradually increases. The slope of the loading curve of cycle 4 is approximately twice than that of the cycle 1. However, in cycle 3 and 4 the slope of the loading and the unloading curve is similar, indicating that there might be a threshold for strain hardening of flax fibers above which there will not be a marked difference in the Young's modulus.

(**a**)   (**b**)
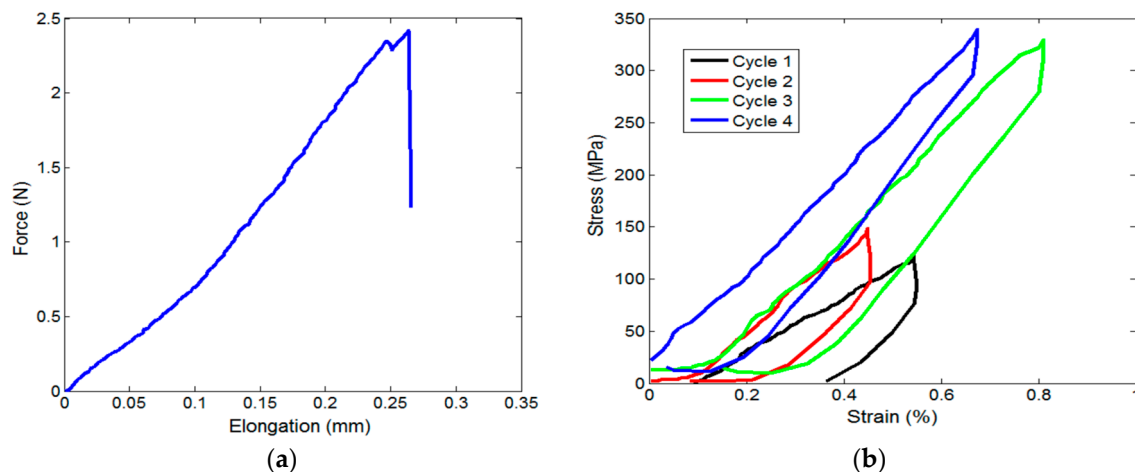
Figure 3. (**a**) Force-Elongation curve and (**b**) hysteresis curve of a technical flax fiber. Area under the force elongation curve represents the total energy absorbed during the fracture. Hysteresis curve shows the gradual increase in modulus during each successive loading unloading cycle.

### 3.1. In Situ Failure Analysis through SEM

SEM movies that were captured reveal three distinct phases of fiber failure, (1) initial rotation of fiber bundle; (2) segregation of the single fibers from the bundle; and (3) ultimate failure of the fiber. (Movie is attached at the supplement).

3.1.1. Initial Rotation of the Fiber Bundle

At the beginning of the application of the tensile load, the technical fiber undergoes a certain degree of rotation as revealed in the movie captured by the SEM. The reason of this rotation of the fiber bundle may be attributed to the presence of the helically arranged micro-fibrils located at the S2 layers within the single fibers. The micro-fibrils in the primary layer are randomly oriented. On the other hand, micro-fibrils in the S1 and S3 layer are arranged in circumferential direction [5]. As a result, micro-fibrils from the primary, S1 and S3 layers have negligible contribution to this rotation effect. This rotation occurs approximately up to 0.3% of the total strain of the fiber. When an axial load is applied to the both ends of a technical fiber, the micro-fibrils within the single fiber tend to straighten and align with the fiber longitudinal axis. However, as the micro-fibrils are not free to move and are naturally adhering to the polysaccharide matrix, the net effect is to impart rotation and twist on the fiber bundle.

#### 3.1.2. Segregation of Single Fibers from the Bundle

As the magnitude of tensile force increases, single fibers are observed to segregate from the bundles adhering together by pectin (Figure 4a). The red arrow indicates segregated region while the yellow arrow indicates intact region (Figure 4a). At this moment, the diameter of the fiber bundle increases which is the result of separation of single fibers. As the force continues to increase, the single fibers tend to slide past one another.

(**a**) (**b**)
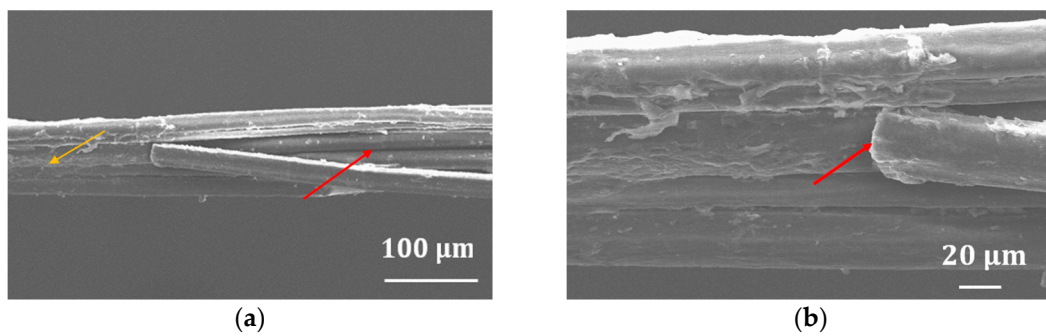
Figure 4. (**a**) Breaking of technical fiber with lower magnification and (**b**) with higher magnification. The single fiber broke with no prior indication of failure. There is limited brooming or bristling at the failed region of the fiber.

3.1.3. Ultimate Failure of the Fiber

It was found in the captured SEM movies that the ultimate failure of a fiber bundle occurs without any prior indication of failure. In a specific fiber bundle, with more or less uniform diameter, it is hard to predict the specific location of failure. This is due to a high variation in the distribution of defects throughout the length of the fiber. It was also found that not all elementary fibers fail at the same time and locations, but rather they fail at different locations and different points in time. After failure, near the fractured area, some elementary fibers within the bundle were seen to bristle or assume a broom like shape as can be seen in Figure 5a. In some other cases, the bundle break with a snapping sound and had limited brooming of the elementary fibers as shown in Figure 4b (red arrow).

(**a**) (**b**)
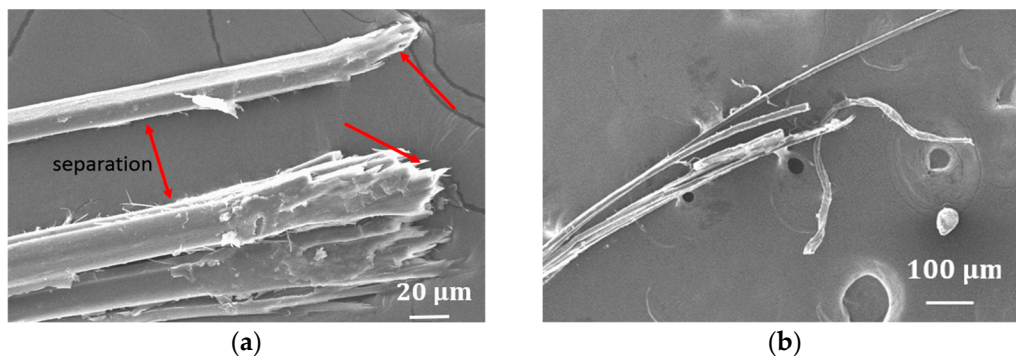
Figure 5. (**a**) Brooming of fiber after failure (red arrow) and (**b**) Individual fibers are seen to break at different region.

3.2. Fractographic Analysis of Single Fibers

Figure 6a,b shows the side view of the fractured surface of a single or elementary flax fiber that failed in tension at a displacement rate of 0.25 mm/min. These two images also reveal some of the intricate details of the elementary flax fiber as the outer surface (may include primary wall as well as S1 layer) is ripped away. The cylindrical shaped meso-fibrils, sometimes erroneously called micro-fibrils in the literature, are exposed. These meso-fibrils reside in S2 layer and have a diameter of 1–2 μm. And the angle these meso-fibrils make with the fiber longitudinal axis is called micro-fibril angle.
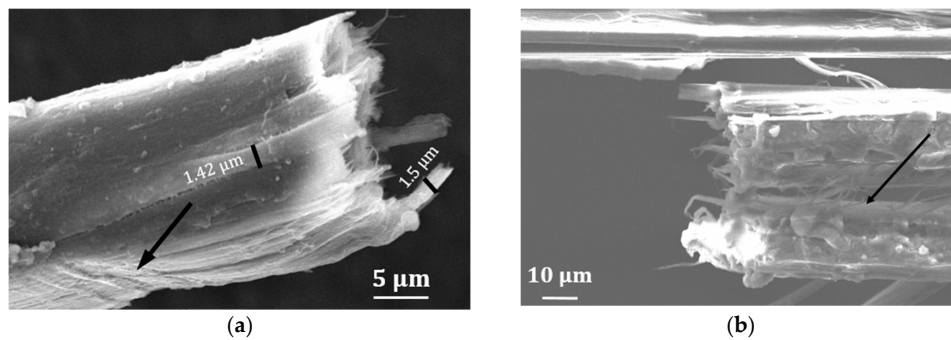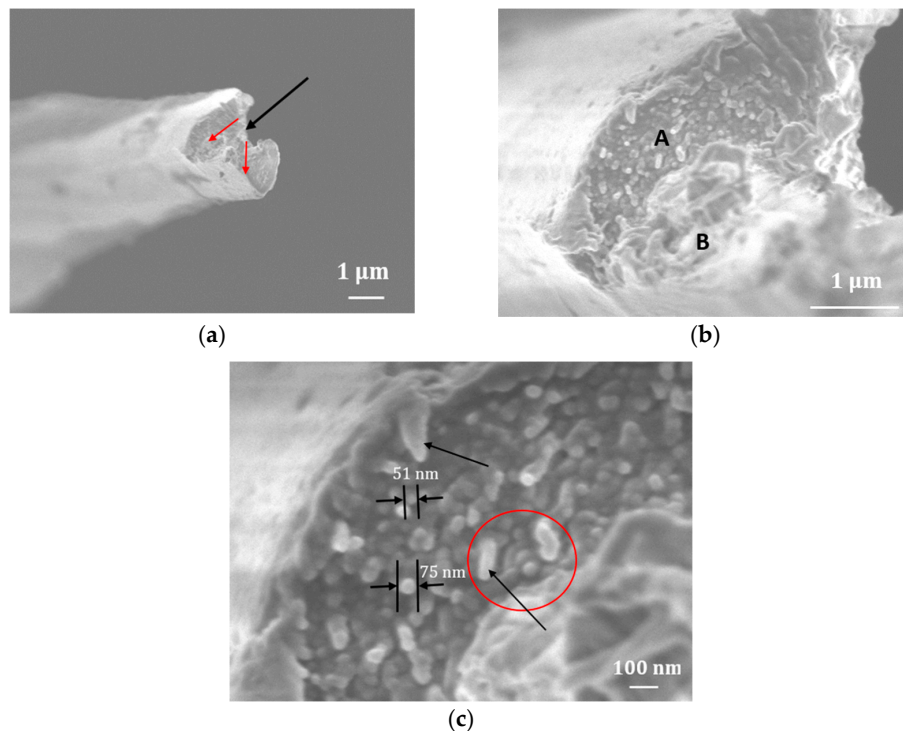
Figure 6. (**a**) Side view of the fractured surface of an elementary flax fiber. Crease on the outer surface is visible (arrow). Individual meso-fibrils are also visible (black bar); (**b**) Meso-fibrils are seen to be aligned with fiber axis after the fibers are exposed to tension until failure.

The fractured surfaces that can be seen in Figure 6a are very rough, which is the characteristics of a tensile failure [35]. On the contrary, in compressive failure, the surfaces are usually flat and shiny [35]. The way the outer surface (arrow) is removed bears the evidence of certain degree of rotation (Figure 6a). In Figure 6b, crack has propagated in the longitudinal direction (arrow) and delamination of the meso-fibrils from the hemicellulose matrix can be observed. The meso-fibrils are seen to be pulled out from the matrix in longitudinal direction (Figure 6a,b) as well as in the transverse direction (Figure 6a). Though these meso-fibrils make an angle of approximately 10° with the longitudinal axis, the angle seem to disappear at the fractured region and the meso-fibrils are almost parallel with the axis (Figure 6b). The dimension of meso-fibril is approximately 1.5 μm (Figure 6a).

Figure 7a–c shows the fracture surface of a meso-fibril. These images were captured when meso-fibrils were exposed after breaking a single fiber with 0.25 mm/min displacement rate. The radial steps or chevron (arrow) indicates the presence of rotational failure (Figure 7a) [36,37]. When a glass fiber is subjected to torsion, a helical crack is created and propagates along the surface. The crack initiates at some defects or voids furthest from the center of the fiber as stress is maximum at that point. This crack propagation usually occurs at 45° angle with respect to the fiber longitudinal axis [36,37]. In other words, due to the applied shear stress, two principal stresses are created in a small element of the fiber: one is compressive and another is tensile. Fracture mainly occurs due to this tensile principal stress [38]. In a similar way, this radial step region might be a potential site for crack initiation and crack propagation. After a crack initiates at that region, it then propagates further downward (red arrow) creating two dissimilar regions: region A and region B (Figure 7b). The roughness of the fractured region often indicates the type of fracture mode dominating the failure [35]. A very rough and highly fibrous surface generally represent tensile failure, and a flat, less fibrous (that is, the end of the fibrils are relatively in the same plane), generally reflects compression failure [35,39]. So the region A is more indicative of a compression failure and region B infers more of tensile failure. It may be perplexing how compressive stress is generated in a tensile specimen. However, this phenomenon is discussed elsewhere in the literature [35,40,41]. When a unidirectional composite is loaded in tension, a compressive stress may generate due to the backward motion of the partially failed region of the fiber in tension. The dynamic stress wave generated in the process may be of such magnitude that it exceeds the compressive strength of the single flax fiber. In this way, a compressive failure may occur and a region of compressive failure may be created in the fiber. This behavior only occurs in unidirectional composite materials that are loaded in tension [39]. As flax fiber is regarded as a natural composite, this type of phenomena would not be uncommon to occur [42]. Again in terms of the speed or velocity of the crack propagation, region A indicates the slower rate of crack propagation. The nano-fibrils in region A have sufficiently more time to break and just sufficient energy to propagate the crack. Therefore, these fibrils reside nearly in the same plane. On the other hand, as the speed of crack propagation increases, there is some surplus energy which causes the fiber to be abruptly

pulled out, and nano-fibrils in region B are no more in the same plane and shows up as rugged surfaces. In addition to these compression and tensile effects, there may have an effect of matrix anisotropy during failure. Meso-fibrils reside in a matrix of hemicellulose and pectin which is highly anisotropic. The anisotropy of the hemicellulose and pectin may arise due to the inhomogeneous deposition of these cell wall polymers during the cell wall formation [43]. The molecular arrangement of hemicellulose and pectin itself are anisotropic. As a result, the matrix of a flax fiber, which is composed of hemicellulose, lignin, and pectin (with different properties), become highly anisotropic. This anisotropy of the matrix may have imparted a twisting moment on the fiber which is evidenced by the presence of the chevron in the radial direction (twisting is also visible in the video).


(**a**) (**b**)

(**c**)

Figure 7. Cross sectional view of the fractured surface of a meso-fibril failed at 0.25 mm/min displacement rate is shown. (**a**) Meso-fibril failure surface is shown and the chevron (arrow) indicates the presence of rotation during failure; (**b**) Magnified view of the same surface is shown. Region A represents low speed crack propagation and region B represents high speed crack propagation; (**c**) Magnified view of the region A is shown, individual microfibrils are observed, micro-compression of these microfibrils can also be seen.

Furthermore, in region A, the end of the micro-fibrils are observed to be microscopically bent (Figure 7c) (circle and arrow), and are not normal to the surface [28]. This is due to the micro-compression of the micro-fibrils [33]. As region A is thought to be in compression, this compressive stress generates an in-plane shear stress which pushes these micro-fibrils sideways rather than being perfectly straight [28].

Figure 8a shows a schematic diagram of the force resolution of a single fiber under tension. When tensile load is applied on both ends of the fiber, part of the load is carried out by the mesofibrils. As mesofibrils make an angle with the loading direction, there exists a horizontal and vertical component. The vertical component superimposes with the loading direction. In an ideal situation, where microfibril angle is same on all over the length of the single fiber, the horizontal component should cancel out each other and there would be no shear stress. However, this is not the case in reality. Figure 8b shows the arrangement of mesofibrils in a single flax fiber (red arrow). It can be seen that they are arranged at an angle with the fiber axis. The two regions in red circles show that the

microfibril angle is not same on all over the length of the single fiber. Moreover, these mesofibrils are not free to move, rather they are embedded on a hemicellulose and pectic matrix. As a result when a tensile load is applied on the fiber, the horizontal component does not cancel out and a shear stress is present which may cause the microbuckling or microcompression of the microfibrils [44].


(**a**)

(**b**)
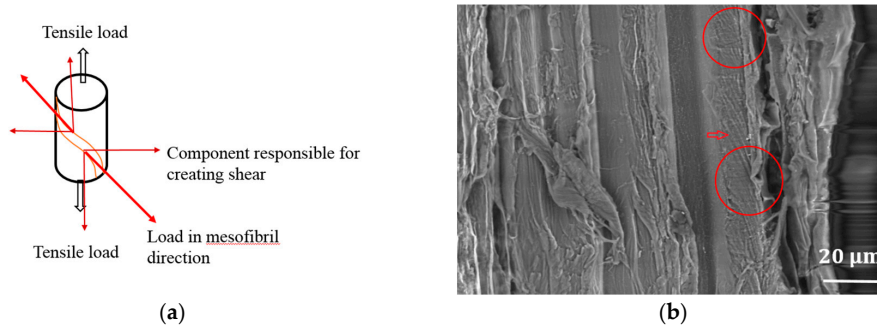
Figure 8. (**a**) Schematic representation of component of forces in a single fiber (**b**) Meso-fibrils (red arrow) are seen to be exposed after the removal of the outer surface. Two circled region shows that microfibril angle is not constant throughout the whole length of the fiber.

Figure 9a shows the fractured region of a meso-fibril that failed at 0.75 mm/min strain rate. Micro-fibrils are observed to stick out form the meso-fibrils in different direction which reflects the high speed of failure. Figure 9b shows the splitting of the fiber end both in longitudinal and cross-sectional direction (red circle and arrow). Evidence of microbuckling or microcompression (due to the presence of shear stress) is also present at the end of these meso-fibrils (red circle). Micro-fibrils are visible in Figure 9c. All of these micro-fibrils got straitened and became parallel to the axis of meso-fibrils after the failure (arrow).

(**a**)

(**b**)

(**c**)
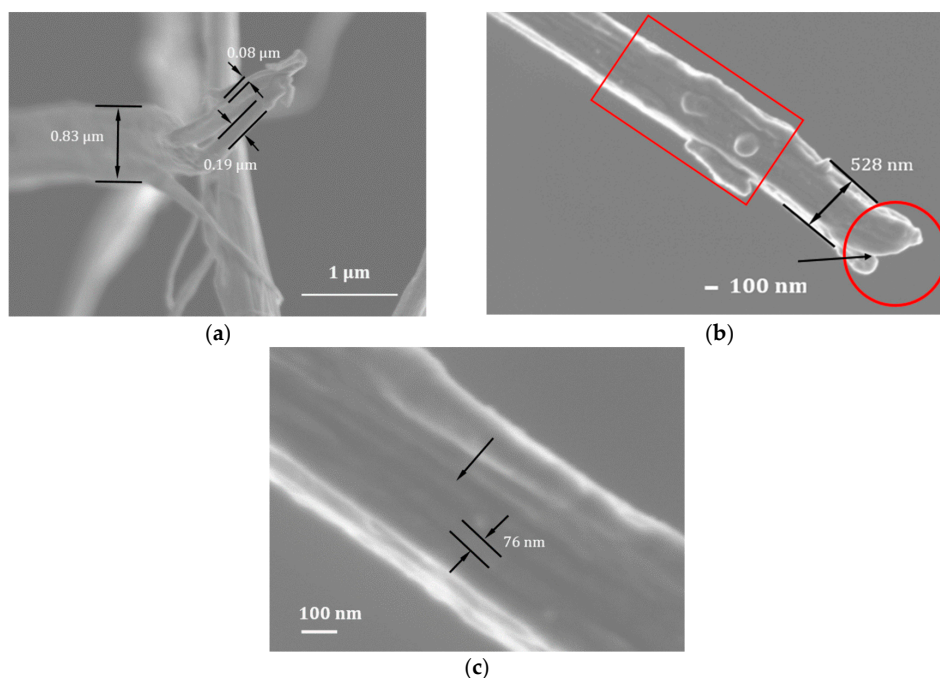
Figure 9. Fractured surfaces of a meso-fibril that failed at 0.75 mm/min displacement rate is shown. (**a**) Micro-fibrils pull out from a meso-fibril can be seen; (**b**) side view of a meso-fibril is shown, traces of matrix element are seen to adhere on the fibril surface (rectangle region); (**c**) magnification of the same meso-fibril is shown, individual micro-fibrils can be seen (arrow) and they are aligned with the meso-fibril axis.

Figure 10a shows the fracture surface of a single flax fiber pulled at 1.6 mm/min displacement rate. The two circles indicate the potential site of crack initiation and the arrow indicates the direction of crack propagation (as flax fibers can be treated as composites) [39]. At the beginning, the velocity of the crack was slow and as a consequence, a relatively smoother surface was created in region A. As the crack continues to propagate, the velocity becomes higher and higher leaving the surface rougher and rougher creating many ridges and rivers in region B [40]. A magnified image is shown in Figure 10b which exposes a crack in region C.

(a)

(b)

(c)

(d)
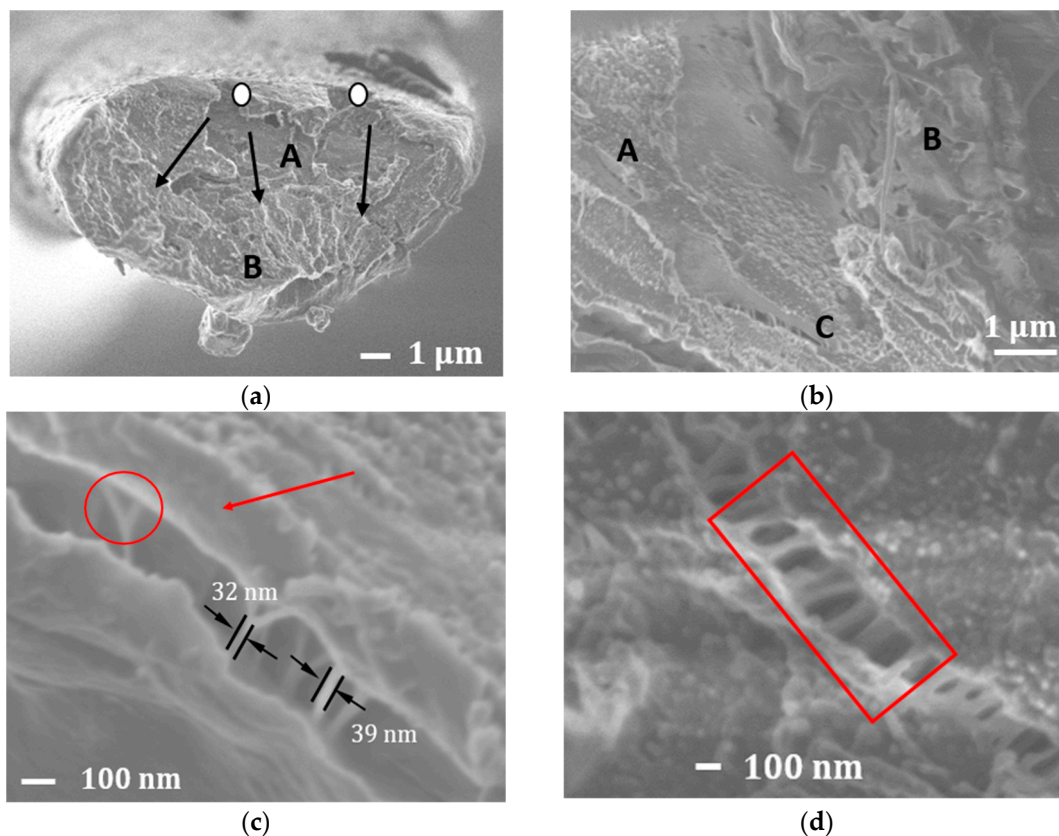
Figure 10. (**a**) Cross sectional view of the fractured surface of an elementary fiber failed at 1.6 mm/min displacement rate is shown. The white circle represents the potential site for crack initiation and the arrow represents the direction of crack propagation; (**b**) Magnified view of the same surface is shown, three distinct regions are visible, region A represents the region of low speed crack propagation, region B represents the high speed crack propagation, region C shows a crack opening; (**c**) Magnified view of region C is shown, bifurcation of microfibrils (red circle) can be observed; (**d**) Crack bridging by microfibrils are observed (rectangled region), microfibrils are at an angle with the crack wake confirming the presence of shear deformation.

A magnified view of region C is shown in Figure 10c. Crack bridging phenomena usually arises in polymer matrix composites where the fiber and the matrix are both brittle [45,46]. This crack bridging reduces the stress intensity factor ahead of the crack tip and thus decreases the possibility for unstable crack propagation. Similar crack bridging phenomena is observed in the failure surface of flax fibers which also suggests the brittle nature of the micro-fibrils and the hemicellulose matrix. In the image (Figure 10c,d), crack bridging by the micro-fibrils can be observed and the micro-fibrils have been pulled out of the hemicellulose matrix [32]. The micro-fibrils seem to bifurcate (Figure 10c, red circle) near the meso-fibrils (red arrow). However, the meso-fibrils are not very clean and significant amount of matrix material is seen to adhere to the meso-fibril surface. This crack bridging phenomena indicates

a poor fiber matrix bond strength of flax fiber. However, this crack bridging by micro-fibrils acts as an energy dissipating mechanism and helps to prevent faster crack propagation in the fiber.

From Figure 10d it is clear that the pulled out micro-fibrils are not perpendicular to the crack wake surface, but rather they are slightly bent (rectangular region). This indicates that certain amount of shear stress is present during the failure as indicated in Figure 8a. It is assumed that the failure mechanism for polymer matrix composites is also applicable for the failure of flax fibers. As a result, with the increase in the angle of inclination these micro-fibrils, the bridging stress would be reduced and the micro-fibrils would no longer be able to resist the faster propagation of crack. However, in flax fiber, the angle of inclination of these micro-fibrils is high enough to achieve a higher bridging stress, thus resisting faster crack propagation and imparting toughness and strength during their fracture.

The work of fracture of flax fiber was calculated to be $2.94 \times (10^6)$ J/m^2 from Figure 3a using the formula provided by Giorgio Jeronimidis [47] which is an order of magnitude higher than the cellulosic single cell of wood (10^5) J/m^2 [48]. This high value of work of fracture of the bundle of single cells of flax fiber is explained by the above fracture surface analysis and can be summarized as follows:

The spiral angle of flax fiber contributes to the energy dissipating mechanism by untwining the angle during tensile testing. A fiber with a higher spiral angle would be tougher as they would untwine during the tensile failure. On the other hand, if the meso-fibrils are perfectly aligned with the fiber axis, the stiffness of the fiber would increase, however, the toughness would be decreased as there would be little untwining during tensile failure.

The hierarchical fiber pull out mechanism contributes to the high work of fracture of flax fibers. That is, initially, after the breakage of the primary wall, meso-fibrils are pulled out of the matrix, then micro-fibrils are pulled out of the mesofibrils. These micro-fibrils, with a diameter of 50–70 nm, might be made of smaller fibrils. These smaller fibrils pull out might also occur which would be subjected to further investigation. It was suggested by G. Jeronimidis and Julian Vincent [49] that if one calculates the toughness of a fibrous composite using the same volume fraction as a wood fiber, the toughness would be ten times less than actually observed from a wood fiber. Because for fibrous composite, the only toughening mechanism is the presence of frictional force during fiber pull-out. However, during hierarchical fiber pull-out of flax fiber, frictional force is coming from different layers.

Crack bridging phenomena also contributes to the high work of fracture of flax fiber. Though the contribution of crack bridging phenomena was not accounted for the high work of fracture of flax fiber in previous study, Figure 10d strongly corroborates their presence during fracture. The microfibrils between the crack wake surfaces participates in the smooth transfer of stress. In addition, for wood cell, it was found that with the decrease in temperature, the toughness increases, which is opposite to most materials [49]. In lower temperature, the fibers would be more viscous which would result in improved transfer of stress to the crack tip and would contribute to the high work of fracture.

4. Tensile Testing of Flax Fibers with Different Strain Rate

Though it is true that, being natural or bio-fibers, the fracture surface of flax fibers would be different from fiber to fiber, however, the general failure mechanism involved during the failure process, such as, hierarchical fiber pull out, untwining of mesofibrils, and crackbridging is common to most fibers. For investigating the effect of strain rate on the strength of flax fibers, 150 technical fibers were tested with a displacement rate of 0.25 mm/min, 0.75 mm/min and 1.6 mm/min which corresponds to a strain rate of 0.01, 0.03 and 0.08 min^{-1}. At least 50 fibers were tested for each displacement rate. Schwartz et al. [50] investigated the effect of strain rate and gauge length on the failure of ultra-high strength polyethylene fibers. For investigating the effect of strain rate, they fixed the gauge length at 50 mm and used the strain rates at 0.004, 0.1, 0.4, and 1 min^{-1}. For investigating the effect of gauge length, they fixed the strain rate at 0.1 min^{-1}, and used the gauge lengths of 10, 50, 100 and 200 mm. They found that with the increase in strain rate, the failure strength increases and the fibers transition from viscoelastic to elastic nature. The failure surface becomes more fibrillated as the strain rate increases. Okoli et al. [51,52] studied the effect of strain rate on fiber reinforced composites (glass

fiber/Epoxy). They found that with the increase in strain rate, the failure strength of the composite increases. They reasoned that this increase stems from the increase in strength of glass fibers from high strain rate, as glass fibers are strain rate sensitive. The amount of energy absorbed during the failure process is also increased with the increase in strain rate.

Table 1 summarizes the results for strain rate testing of flax fibers in this study. Flax fibers, being natural polymeric materials, are expected to show strain rate sensitivity. However, the mean of these three sets of samples is not statistically significant. That is, the strain rate sensitivity is not observed within the specified limit of strain rate tested. One reason for this behavior is that the strain rate used in this experiment (0.01–0.08 min^{-1}) does not vary appreciably that would produce the increase in failure strength. For the strain rate 0.01 min^{-1}, the failure strength of flax fibers showed very limited scatter and the range is very short. The highest range of failure strength is observed with the strain rate of 0.03 min^{-1}. With regards to glass fiber, Cansfield et al. [53] found that the strain rate of 0.2 min^{-1} (3.10^{-3} s^{-1}) is the threshold at which the glass fibers starts to show appreciable increase in strength. At this strain rate (0.2 min^{-1}), the distinct yield point which is visible on stress-strain curve starts to disappear.

Table 1. Summary of the results of tensile testing with different strain rate.

| Strain Rate	0.01 min^{-1}	0.03 min^{-1}	0.08 min^{-1}
Failure strength (MPa)	389 ± 203	637 ± 414	364 ± 244
Failure strain (%)	1.055 ± 0.24	0.93 ± 0.29	1.02 ± 0.31
Elastic modulus (GPa)	37 ± 20	60 ± 31	38 ± 20
Failure time (Second)	55 ± 18	15 ± 4.6	8.2 ± 2.24
Number of discard	2	5	8

Figure 11a–d shows the distribution of failure strength, failure strain, elastic modulus and failure time of technical flax fibers at three different strain rates, namely 0.01 min^{-1}, 0.03 min^{-1} and 0.08 min^{-1}. For all box and whisker plots in this study, the red line represents the median. The blue box represents the interquartile range (IQR). The whiskers at the lower and upper end represent the span of all the data points, that is, the range of the data points. Generally, when the data points lie outside the 1.5 times the interquartile range (IQR), they are defined as the outliers. However, due to the relatively small data sets (50 specimens for each strain rate), no values were removed as outliers. All the data points were taken into consideration for calculating the mean and standard deviation [54].

It is often useful to quantify the dispersion or spread of the data with the help of statistical distributions. Weibull distribution is one of the most widely used statistical distribution for predicting the probability of failure of brittle materials [55]. The cumulative distribution function of Weibull distribution can be expressed in the following ways

$$F(\sigma) = 1 - \exp\left[-\left(\frac{\sigma}{\sigma_0}\right)^m\right] \tag{1}$$

where

$$F(\sigma) = \text{ Probability of failure}$$
$$\sigma = \text{ Applied stress}$$
$$\sigma_0 = \text{ Scale parameter or scale factor}$$
$$m = \text{ Shape parameter or shape factor or Weibull modulus}$$
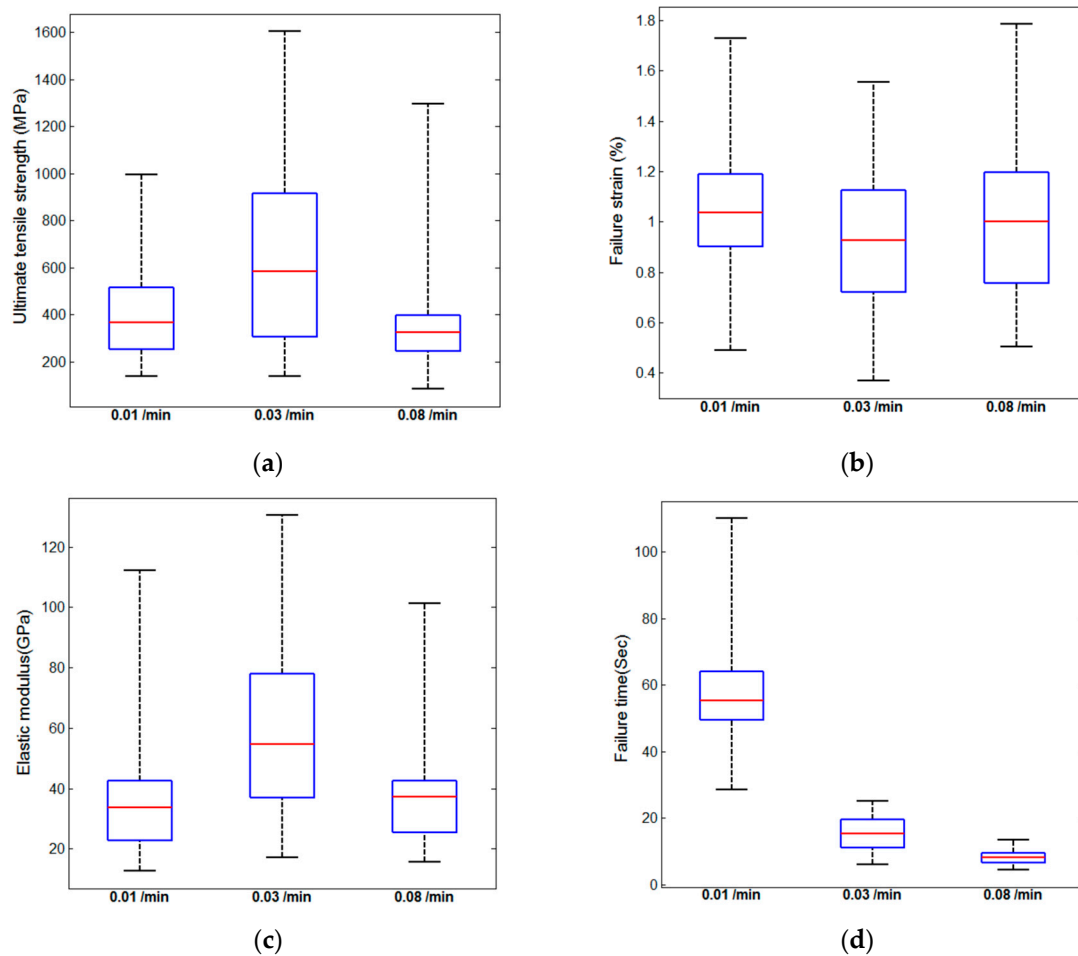
Figure 11. (**a**) Distribution of ultimate tensile strength; (**b**) failure strain; (**c**) elastic modulus; and (**d**) failure time of flax fibers with three different strain rates, namely 0.01/min, 0.03/min, and 0.08/min.

This distribution is based on the weakest link theory, which assumes that failure occurs at the weakest point of a body. As the volume or length of the structure increases, the probability of failure also increases. The value of *m* provides a quantitative estimate of the spread or dispersion of the data. A higher *m* value represents that the data are closely spaced and possess low standard deviation, which is the case for ductile materials. On the other hand, a lower *m* value represents that the data are widely spaced and possess a higher standard deviation, which is the case for brittle materials. As flax fibers fail in a brittle manner, Weibull distribution is appropriate for quantifying the dispersion of these fibers.

A bundle of flax fiber is usually referred to as the technical fiber and an individual fiber is called a single fiber or fiber ultimate or elementary fibers. Into a technical fiber, these single fibers are held together by pectic polysaccharides. The strength of the elementary fibers was reported to be higher than the technical fibers. With the increase in gauge length, the strength of elementary fibers was reported to decrease. This phenomenon is due to the number of defects present in the single fibers. As the gauge length of the fiber increases, the number of defects present in the fiber also increases, which reduces the strength of the fiber. The defects in the elementary fibers are generally referred to as kink bands, dislocations or nodes [56] (Figure 12a). They are actually localized distortions of the cell wall. More specifically, when the meso-fibrils in the secondary cell wall get misaligned and oriented perpendicular to the fiber axis, the region is slightly protruded from the plane surface, and they can be seen in plane polarized microscope as thin strips or dark lines. They may originate during the growth or processing (hackling, scutching, and separating) of the fibers. These kink bands are the

weakest points in the elementary fiber. During tensile testing, the origin and propagation of cracks occur from these kink bands. The amount of damage sustained by the elementary fiber is usually quantified by the presence of the kink bands per unit length. The number of kink bands in a single fiber may vary between 100 and 500 [57], and the spacing between the two adjacent kink bands may be approximately 120 micrometer [58]. Figure 12a shows the presence of kink bands or dislocations on a single flax fiber which are regarded as the weakest points in the fiber. Figure 12b shows the probability of failure of technical flax fibers with two different strain rates, namely 0.01 min^{-1} and 0.03 min^{-1}. The data were fitted with two parameter Weibull distribution and the parameters of the distribution were determined using the maximum likelihood method. For a 95% confidence interval (CI), the *m* value of the Weibull distribution for 0.01 min^{-1} strain rate is 2.1238 while the *m* value for 0.03 min^{-1} strain rate is 1.74, which means that the data for 0.03 min^{-1} strain rate has a higher dispersion. Table 2 presents a more detailed analysis of the shape parameters and scale parameters of the three strain rates tested in this study.
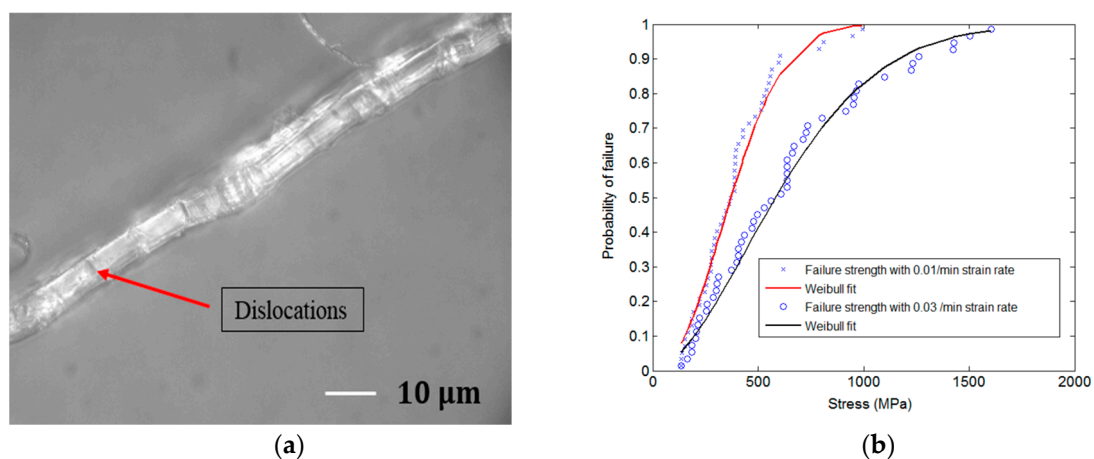
Figure 12. (**a**) Dislocations or kink bands on single flax fiber; (**b**) Weibull distribution fit of the data with two different strain rates.

Table 2. Summary of the results of different parameters of Weibull distribution.

Strain Rate	Shape Parameter (Best Fit)	Scale Parameter (Best Fit)	[Lower Bound, Upper Bound] of Scale Parameter for 95% CI	[Lower Bound, Upper Bound] of Shape Parameter for 95% CI
0.01 min^{-1}	2.1238	441.3294	[384.8261, 206.1290]	[1.7366, 2.5972]
0.03 min^{-1}	1.7400	719.2087	[607.6565, 851.2394]	[1.4050, 2.1548]
0.08 min^{-1}	1.8013	412.6898	[350.4343, 486.0050]	[1.4936, 2.1723]

5. Conclusions

The dynamic failure of flax fiber was investigated with the help of SEM movie while the fiber was being pulled in tension. Three distinct phases of fiber failure were identified. The fractographic analysis of the failure surface of single fibers and meso-fibrils was performed in detail. It was proposed that the spiral angle, hierarchical fiber pull out, and crack bridging- all contribute to the high work of fracture of flax fiber. The fractographic approach of the failure of flax fiber reveals some of the intricate details of the structure of flax fiber such as the arrangement of mesofibrils and microfibrils, and also supports the findings of Thuault et al. [13] about the presence of more than four layers in flax fibers. The strain rate sensitivity of technical flax fibers on the mechanical properties of flax fibers such as, failure strength, failure strain, elastic modulus, and failure time with three different strain rates namely, 0.01, 0.03 and 0.08 min^{-1} was investigated. The data were presented in the form of boxplot representation. A 2-parameter Weibull distribution analysis on the data were also performed

to quantify the spread or dispersion of the data points and to predict the probability of failure with applied stress.

From an application point of view, the investigation on the failure mechanism of flax fiber is important as it provides insight into manufacturing of bio-mimetic and bio-mimicking novel composite materials [59]. Flax fibers are essentially polymer-polymer composite materials. The understanding and knowledge gained from this study regarding the energy dissipating mechanism of flax fibers may inspire the improvement of design principles for technical composite materials.

Flax fibers are shown to be stiff and tough at the same time. A few recent works [42,60,61] suggest that to achieve these two contradicting properties in composite materials, a tight interface between the stiff fiber and soft matrix is required. In flax fiber, the hemicellulose molecules act as these interface polymers. Because the chemical nature of hemicellulose is similar to cellulose, they can form a strong non-covalent bond. On the other hand, the hemicellulose, being extremely hydrophilic, can form a gel-like hydrated network with pectin which is necessary for imparting toughness. As explained previously, this gel-like matrix is able to flow plastically without fracturing beyond their yield stress [62]. The interface of technical composite materials can be improved by learning from these natural composite materials, such as wood fiber [63] and flax fiber. By selecting appropriate amphiphilic molecules or surfactants, it is possible to achieve a strong bond between an aqueous and a hydrophobic phase, thus improving the interfacial strength of composite materials.

Author Contributions: Shabbir Ahmed prepared the sample, carried out the experiment, analyzed data, and drafted the manuscript. Chad A. Ulven supervised and guided the overall project and involved in drafting the manuscript.

Conflicts of Interest: The authors declare no conflict of interest.

References

1. Bledzki, A.; Gassan, J. Composites reinforced with cellulose based fibres. *Prog. Polym. Sci.* **1999**, *24*, 221–274. [CrossRef]
2. Fuqua, M.A.; Huo, S.; Ulven, C.A. Natural fiber reinforced composites. *Polym. Rev.* **2012**, *52*, 259–320. [CrossRef]
3. Morvan, C.; Andème-Onzighi, C.; Girault, R.; Himmelsbach, D.S.; Driouich, A.; Akin, D.E. Building flax fibres: More than one brick in the walls. *Plant Physiol. Biochem.* **2003**, *41*, 935–944. [CrossRef]
4. Romhany, G.; Karger-Kocsis, J.; Czigany, T. Tensile fracture and failure behavior of technical flax fibers. *J. Appl. Polym. Sci.* **2003**, *90*, 3638–3645. [CrossRef]
5. Gibson, L.J. The hierarchical structure and mechanics of plant materials. *J. R. Soc. Interface* **2012**. [CrossRef] [PubMed]
6. Domenges, B.; Charlet, K. Direct insights on flax fiber structure by focused ion beam microscopy. *Microsc. Microanal.* **2010**, *16*, 175–182. [CrossRef] [PubMed]
7. Cosgrove, D.J. Assembly and enlargement of the primary cell wall in plants. *Ann. Rev. Cell Dev. Biol.* **1997**, *13*, 171–201. [CrossRef] [PubMed]
8. Carpita, N.C.; Gibeaut, D.M. Structural models of primary cell walls in flowering plants: Consistency of molecular structure with the physical properties of the walls during growth. *Plant J.* **1993**, *3*, 1–30. [CrossRef] [PubMed]
9. Adler, E. Lignin chemistry—Past, present and future. *Wood Sci. Technol.* **1977**, *11*, 169–218. [CrossRef]
10. Rose, J.K. *The Plant Cell Wall*; CRC Press: Boca Raton, FL, USA, 2003; Volume 8.
11. Peterlin, A.; Ingram, P. Morphology of secondary wall fibrils in cotton. *Text. Res. J.* **1970**, *40*, 345–354. [CrossRef]

12. Baley, C.; Le Duigou, A.; Bourmaud, A.; Davies, P. Influence of drying on the mechanical behaviour of flax fibres and their unidirectional composites. *Compos. Part A Appl. Sci. Manuf.* **2012**, *43*, 1226–1233. [CrossRef]

13. Thuault, A.; Domengès, B.; Hervas, I.; Gomina, M. Investigation of the internal structure of flax fibre cell walls by transmission electron microscopy. *Cellulose* **2015**, *22*, 3521–3530. [CrossRef]

14. Goudenhooft, C.; Siniscalco, D.; Arnould, O.; Bourmaud, A.; Sire, O.; Gorshkova, T.; Baley, C. Investigation of the Mechanical Properties of Flax Cell Walls during Plant Development: The Relation between Performance and Cell Wall Structure. *Fibers* **2018**, *6*, 6. [CrossRef]

15. Roach, M.J.; Mokshina, N.Y.; Badhan, A.; Snegireva, A.V.; Hobson, N.; Deyholos, M.K.; Gorshkova, T.A. Development of cellulosic secondary walls in flax fibers requires β-galactosidase. *Plant Physiol.* **2011**, *156*, 1351–1363. [CrossRef] [PubMed]

16. Mikshina, P.; Chernova, T.; Chemikosova, S.; Ibragimova, N.; Mokshina, N.; Gorshkova, T. Cellulosic fibers: Role of matrix polysaccharides in structure and function. In *Cellulose-Fundamental Aspects*; InTech: Vienna, Austria, 2013.

17. Ding, S.-Y.; Liu, Y.-S.; Zeng, Y.; Himmel, M.E.; Baker, J.O.; Bayer, E.A. How does plant cell wall nanoscale architecture correlate with enzymatic digestibility? *Science* **2012**, *338*, 1055–1060. [CrossRef] [PubMed]

18. Müller, M.; Czihak, C.; Vogl, G.; Fratzl, P.; Schober, H.; Riekel, C. Direct observation of microfibril arrangement in a single native cellulose fiber by microbeam small-angle X-ray scattering. *Macromolecules* **1998**, *31*, 3953–3957. [CrossRef]

19. Astley, O.M.; Donald, A.M. A small-angle X-ray scattering study of the effect of hydration on the microstructure of flax fibers. *Biomacromolecules* **2001**, *2*, 672–680. [CrossRef] [PubMed]

20. Bourmaud, A.; Morvan, C.; Bouali, A.; Placet, V.; Perre, P.; Baley, C. Relationships between micro-fibrillar angle, mechanical properties and biochemical composition of flax fibers. *Ind. Crops Prod.* **2013**, *44*, 343–351. [CrossRef]

21. Baley, C. Analysis of the flax fibres tensile behaviour and analysis of the tensile stiffness increase. *Compos. Part A Appl. Sci. Manuf.* **2002**, *33*, 939–948. [CrossRef]

22. Hearle, J. The fine structure of fibers and crystalline polymers. III. Interpretation of the mechanical properties of fibers. *J. Appl. Polym. Sci.* **1963**, *7*, 1207–1223. [CrossRef]

23. Charlet, K.; Jernot, J.-P.; Gomina, M.; Bizet, L.; Bréard, J. Mechanical properties of flax fibers and of the derived unidirectional composites. *J. Compos. Mater.* **2010**, *44*, 2887–2896. [CrossRef]

24. Bos, H.; Van Den Oever, M.J.; Peters, O.C. Tensile and compressive properties of flax fibres for natural fibre reinforced composites. *J. Mater. Sci.* **2002**, *37*, 1683–1692. [CrossRef]

25. Shah, D.U.; Nag, R.K.; Clifford, M.J. Why do we observe significant differences between measured and 'back-calculated' properties of natural fibres? *Cellulose* **2016**, *23*, 1481–1490. [CrossRef]

26. Andersons, J.; Spārniņš, E.; Joffe, R.; Wallström, L. Strength distribution of elementary flax fibres. *Compos. Sci. Technol.* **2005**, *65*, 693–702. [CrossRef]

27. Andersons, J.; Poriķe, E.; Spārniņš, E. The effect of mechanical defects on the strength distribution of elementary flax fibres. *Compos. Sci. Technol.* **2009**, *69*, 2152–2157. [CrossRef]

28. McLaughlin, E.C.; Tait, R.A. Fracture mechanism of plant fibres. *J. Mater. Sci.* **1980**, *15*, 89–95. [CrossRef]

29. Nilsson, T.; Gustafsson, P.J. Influence of dislocations and plasticity on the tensile behaviour of flax and hemp fibres. *Compos. Part A Appl. Sci. Manuf.* **2007**, *38*, 1722–1728. [CrossRef]

30. Thygesen, L.G.; Asgharipour, M.R. The effects of growth and storage conditions on dislocations in hemp fibres. *J. Mater. Sci.* **2008**, *43*, 3670–3673. [CrossRef]

31. Davies, G.C.; Bruce, D.M. Effect of environmental relative humidity and damage on the tensile properties of flax and nettle fibers. *Text. Res. J.* **1998**, *68*, 623–629. [CrossRef]

32. Bos, H.; Donald, A. In situ ESEM study of the deformation of elementary flax fibres. *J. Mater. Sci.* **1999**, *34*, 3029–3034. [CrossRef]

33. Mott, L.; Shaler, S.M.; Groom, L.H.; Liang, B.-H. The tensile testing of individual wood fibers using environmental scanning electron microscopy and video image analysis. *Tappi J.* **1995**, *78*, 143–148.

34. Bos, H.L. *The Potential of Flax Fibres as Reinforcement for Composite Materials*; Technische Universiteit Eindhoven Eindhoven: Eindhoven, The Netherlands, 2004.

35. Clements, L.L. Fractography of unidirectional graphite-epoxy as a function of moisture, temperature and specimen quality. *J. Mater. Sci.* **1986**, *21*, 1853–1862. [CrossRef]

36. McCoy, R. SEM fractography and failure analysis of nonmetallic materials. *J. Fail. Anal. Prev.* **2004**, *4*, 58–64. [CrossRef]

37. Slámečka, K.; Šesták, P.; Vojtek, T.; Kianicová, M.; Horníková, J.; Šandera, P.; Pokluda, J. A Fractographic Study of Bending/Torsion Fatigue Failure in Metallic Materials with Protective Surface Layers. *Adv. Mater. Sci. Eng.* **2016**, *2016*. [CrossRef]

38. Quinn, G.D. *Fractography of Ceramics and Glasses*; National Institute of Standards and Technology: Washington, DC, USA, 2007.

39. Greenhalgh, E. *Failure Analysis and Fractography of Polymer Composites*; Elsevier: Amsterdam, The Netherlands, 2009.

40. Clements, L.L. Reply to comment on "Fractography of unidirectional graphite-epoxy as a function of moisture, temperature and specimen quality". *J. Mater. Sci. Lett.* **1989**, *8*, 618. [CrossRef]

41. Purslow, D. Comment on "Fractography of unidirectional graphite-epoxy as a function of moisture, temperature and specimen quality". *J. Mater. Sci. Lett.* **1989**, *8*, 617. [CrossRef]

42. Fratzl, P.; Burgert, I.; Gupta, H.S. On the role of interface polymers for the mechanics of natural polymeric composites. *Phys. Chem. Chem. Phys.* **2004**, *6*, 5575–5579. [CrossRef]

43. Baskin, T.I. Anisotropic expansion of the plant cell wall. *Annu. Rev. Cell Dev. Biol.* **2005**, *21*, 203–222. [CrossRef] [PubMed]

44. Hughes, M.; Sèbe, G.; Hague, J.; Hill, C.; Spear, M.; Mott, L. An investigation into the effects of micro-compressive defects on interphase behaviour in hemp-epoxy composites using half-fringe photoelasticity. *Compos. Interfaces* **2000**, *7*, 13–29. [CrossRef]

45. Leung, C.K.; Li, V.C. Effect of fiber inclination on crack bridging stress in brittle fiber reinforced brittle matrix composites. *J. Mech. Phys. Solids* **1992**, *40*, 1333–1362. [CrossRef]

46. Cartié, D.D.; Cox, B.; Fleck, N. Mechanisms of crack bridging by composite and metallic rods. *Compos. Part A Appl. Sci. Manuf.* **2004**, *35*, 1325–1336. [CrossRef]

47. Jeronimides, G. The fracture of wood in relation to its structure. *Leiden Bot. Ser.* **1976**, *3*, 253–265.

48. Gordon, J.; Jeronimidis, G. Work of fracture of natural cellulose. *Nature* **1974**, *252*, 116. [CrossRef]

49. Vincent, J.F. *Structural Biomaterials*; Princeton University Press: Princeton, NJ, USA, 2012.

50. Schwartz, P.; Netravali, A.; Sembach, S. Effects of strain rate and gauge length on the failure of ultra-high strength polyethylene fibers. *Text. Res. J.* **1986**, *56*, 502–508. [CrossRef]

51. Okoli, O.; Smith, G. Failure modes of fibre reinforced composites: The effects of strain rate and fibre content. *J. Mater. Sci.* **1998**, *33*, 5415–5422. [CrossRef]

52. Huang, W.; Xu, W.; Xia, Y. Effect of strain rate on the mechanical behaviors of SiC fiber. *J. Mater. Sci.* **2005**, *40*, 465–468. [CrossRef]

53. Cansfield, D.; Ward, I.; Woods, D.; Buckley, A.; Pierce, J.; Wesley, J. Tensile-Strength of Ultra High Modulus Linear Polyethylene Filaments. *Polym. Commun.* **1983**, *24*, 130–131.

54. Alcock, M.; Ahmed, S.; DuCharme, S.; Ulven, C.A. Influence of Stem Diameter on Fiber Diameter and the Mechanical Properties of Technical Flax Fibers from Linseed Flax. *Fibers* **2018**, *6*, 10. [CrossRef]

55. Ahmed, S. *Mechanical and Surface Properties of Technical and Single Flax Fiber in Micro and Nano Scale*; North Dakota State University: Fargo, North Dakota, 2017.

56. Andersons, J.; Spārniņš, E.; Poriķe, E. Strength and damage of elementary flax fibers extracted from tow and long line flax. *J. Compos. Mater.* **2009**, *43*, 2653–2664. [CrossRef]

57. Khalili, S.; AKIN, D.E.; Pettersson, B.; Henriksson, G. Fibernodes in flax and other bast fibers. *J. Appl. Bot.* **2002**, *76*, 133–138.

58. Baley, C. Influence of kink bands on the tensile strength of flax fibers. *J. Mater. Sci.* **2004**, *39*, 331–334. [CrossRef]

59. Fratzl, P. Biomimetic materials research: What can we really learn from nature9s structural materials? *J. R. Soc. Interface* **2007**, *4*, 637–642. [CrossRef] [PubMed]

60. Gao, H.; Ji, B.; Jäger, I.L.; Arzt, E.; Fratzl, P. Materials become insensitive to flaws at nanoscale: Lessons from nature. *Proc. Natl. Acad. Sci. USA* **2003**, *100*, 5597–5600. [CrossRef] [PubMed]

61. Jäger, I.; Fratzl, P. Mineralized collagen fibrils: A mechanical model with a staggered arrangement of mineral particles. *Biophys. J.* **2000**, *79*, 1737–1746. [CrossRef]

62. Burgert, I.; Dunlop, J.W. Micromechanics of cell walls. In *Mechanical Integration of Plant Cells and Plants*; Springer: Berlin, Germany, 2011; pp. 27–52.

63. Navi, P.; Rastogi, P.K.; Gresse, V.; Tolou, A. Micromechanics of wood subjected to axial tension. *Wood Sci. Technol.* **1995**, *29*, 411–429. [CrossRef]